Development of a High-throughput NanoBRET Screening Platform to Identify Modulators of the RAS/RAF Interaction

David E. Durrant[1], Emily A. Smith[2,3], Ekaterina I. Goncharova[2,4], Nirmala Sharma[2], Patrick A. Alexander[5], Andrew G. Stephen[5], Curtis J. Henrich[2,3], and Deborah K. Morrison[1]

ABSTRACT

Activating mutations in *RAS* are found in approximately 30% of human cancers, resulting in the delivery of a persistent signal to critical downstream effectors that drive tumorigenesis. RAS-driven malignancies respond poorly to conventional cancer treatments and inhibitors that target RAS directly are limited; therefore, the identification of new strategies and/or drugs to disrupt RAS signaling in tumor cells remains a pressing therapeutic need. Taking advantage of the live-cell bioluminescence resonance energy transfer (BRET) methodology, we describe the development of a NanoBRET screening platform to identify compounds that modulate binding between activated KRAS and the CRAF kinase, an essential effector of RAS that initiates ERK cascade signaling. Using this strategy, libraries containing synthetic compounds, targeted inhibitors, purified natural products, and natural product extracts were evaluated. These efforts resulted in the identification of compounds that inhibit RAS/RAF binding and in turn suppress RAS-driven ERK activation, but also compounds that have the deleterious effect of enhancing the interaction to upregulate pathway signaling. Among the inhibitor hits identified, the majority were compounds derived from natural products, including ones reported to alter KRAS nanoclustering (ophiobolin A), to impact RAF function (HSP90 inhibitors and ROS inducers) as well as some with unknown targets and activities. These findings demonstrate the potential for this screening platform in natural product drug discovery and in the development of new therapeutic agents to target dysregulated RAS signaling in human disease states such as cancer.

Introduction

The RAS GTPases, which include HRAS, KRAS, and NRAS, are among the most prevalent drivers of human cancer, with approximately 30% of tumors harboring an oncogenic *RAS* allele (1). The prominent role of the RAS proteins in tumorigenesis is not surprising given the importance of RAS-driven signaling in the control of cell proliferation. In response to normal growth signals, receptor tyrosine kinases routinely engage guanine nucleotide exchange factors to promote the conversion of RAS to its active GTP-bound state (2). Once activated, RAS interacts with critical downstream effectors such as the RAF kinases (ARAF, BRAF, and CRAF) to further propagate the signal. Following signal transmission, GTPase-activating proteins (GAP) facilitate the conversion of RAS back to its inactive GDP-bound state (2). However, in the case of oncogenic RAS proteins, cancer-associated mutations often cause structural changes that disrupt GAP binding or reduce the intrinsic GTPase activity of RAS (3), resulting in constitutive effector engagement and the constant delivery of signals that promote tumor initiation and maintenance.

It is well established that for mutant RAS proteins to exert their full oncogenic potential, they must interact with the RAF kinases to engage the ERK cascade (4, 5). RAS binding recruits autoinhibited RAF monomers from the cytosol to the plasma membrane, where they become activated through a mechanism that involves relief of autoinhibition and dimerization (6). In RAS-dependent signaling, CRAF/BRAF heterodimers appear to predominate and form highly active dimeric complexes that promote the sequential activation of the downstream MEK and ERK kinases (7). Importantly, it has been shown that RAS-mediated ERK activation can be blocked when RAS/RAF binding is disrupted through mutational events or by the expression of peptides or proteins that encode key regions of the RAS-binding domain (RBD) of RAF (8–10).

Recently, our group has used the bioluminescence resonance energy transfer (BRET) methodology to further investigate the RAS/RAF interaction in live cells (11). This work revealed previously unknown binding preferences among the RAS and RAF family members and demonstrated the marked sensitivity of the assay in detecting changes in RAS/RAF binding. Importantly, the BRET assay preserves the spatial environments of a live cell as well as pathway regulation, thus it has the potential to detect both direct and indirect inhibitors of RAS or RAF function. Taking advantage of this methodology, here, we describe the development and use of a BRET-based screening platform to identify compounds that can modulate RAS/RAF binding in living cells. The libraries evaluated included ones containing synthetic compounds and targeted inhibitors, as well as those comprised of purified natural products or natural product extracts. Through these efforts both inhibitors and enhancers of this critical interaction were

[1]Laboratory of Cell and Developmental Signaling, NCI, Frederick, Maryland. [2]Molecular Targets Program, Center of Cancer Research, NCI, Frederick, Maryland. [3]Basic Research Program, Leidos Biomedical Research, Inc., Frederick, Maryland. [4]Biomedical Informatics and Data Science Directorate, NCI, Frederick, Maryland. [5]NCI RAS Initiative, Cancer Research Technology Program, Frederick National Laboratory for Cancer Research, Leidos Biomedical Research, Inc., Frederick, Maryland.

Note: Supplementary data for this article are available at Molecular Cancer Therapeutics Online (http://mct.aacrjournals.org/).

Corresponding Authors: Deborah K. Morrison, Laboratory of Cell and Developmental Signaling, NCI, Frederick, MD 21702. Phone: 301-846-1733; E-mail: morrisod@mail.nih.gov; and Curtis J. Henrich, curtis.henrich2@nih.gov

Mol Cancer Ther 2021;20:1743–54

doi: 10.1158/1535-7163.MCT-21-0175

This open access article is distributed under Creative Commons Attribution-NonCommercial-NoDerivatives License 4.0 International (CC BY-NC-ND).

©2021 The Authors; Published by the American Association for Cancer Research

identified, demonstrating the potential of this methodology to discover and characterize new agents for targeting RAS-driven malignancies.

Materials and Methods

Cell lines and reagents

293FT and reconstituted RAS-deficient mouse embryo fibroblasts (MEF) were cultured in DMEM supplemented with 10% FBS, 2 mmol/L L-glutamine, and 1% penicillin/streptomycin. MCF10A cells and those stably expressing $KRAS^{G12V}$ were cultured in DMEM/F12 supplemented with 5% horse serum, 0.5 μg/mL hydrocortisone, 20 ng/mL EGF, 100 ng/mL cholera toxin, 10 μg/mL insulin, and 1% penicillin/streptomycin. All cells were grown at 37°C under 5% CO_2. 293FT (catalog no. PTA-5077, RRID:CVCL_6911) and MCF10A (catalog no. CRL-10317, RRID:CVCL_0598) cells were purchased from ATCC. Reconstituted RAS-deficient MEFs were obtained from and sequenced by the NCI-RAS Initiative to confirm the loss of all endogenous RAS proteins and subsequent integration of the $KRAS^{Q61R}$ or $BRAF^{V600E}$ alleles. All cell lines were confirmed to be *Mycoplasma* negative using the MycoAlert kit (Lonza).

The LOPAC library of known bioactive compounds was from Sigma. Other synthetic and pure natural products were obtained from the Drug Synthesis and Chemistry Branch, NCI-Developmental Therapeutics Program (DTP, Frederick, MD) and from the NCI-Molecular Targets Program. Natural product extracts were obtained from the Natural Products Support Group NCI-DTP. CMLD compounds were provided by the Boston University Center for Molecular Discovery (Boston, MA; ref. 12). Antibodies, key reagents, and DNA constructs used in this study are listed in Supplementary Table S1.

NanoBRET assay

The NanoBRET protocol was adapted from the technical manual provided in the Promega NanoBRET Protein:Protein Interaction System. For assay validation, 293FT cells were plated at a density of 4×10^5 cells per well of a 6-well dish, and for screening purposes, cells were plated at a density of 2×10^6 cells per 10 cm dish. The next day, cells were transfected using the X-tremeGENE9 transfection reagent per the manufacturer's instructions, using a 2:1 ratio of X-tremeGENE9 to DNA. For the DNA constructs, an acceptor to donor ratio of 5:1 was used (125 ng pCMV-Halo-$KRAS^{Q61R}$ and 25 ng pCMV-Nano-$CRAF^{WT}$ per 10 cm dish or 25 ng pCMV-Halo-$KRAS^{Q61R}$ and 5 ng pCMV-Nano-$CRAF^{WT}$ per well of a 6-well plate). A total of 24 hours after transfection, cells were trypsinized, washed in complete media, and resuspended in OptiMEM containing 4% FBS at a concentration of 1.1×10^5 cells per mL. HaloTag 618 ligand was then added to the cell suspension (1 μL/mL), and 36 μL of the cell mixture was plated per well of a 384-well white-walled tissue culture plate using a μFill dispenser (BioTek), prior to incubation at 37°C. The next day, 10× stocks of each drug were prepared in phenol-free medium. A total of 4 μL of the 10× drug stock was then added to the appropriate wells using the Biomek FX liquid handler to yield a final volume of 40 μL. For a vehicle control, DMSO was diluted in media and added to cells to make a final concentration of 0.4% DMSO. Plates were incubated with drug for 4 hours at 37°C. To measure BRET, the Nano-Glo substrate was diluted into phenol-free medium (10 μL/mL) and 10 μL of the mixture was added to each well, following which the liquid volumes were mixed for 60 seconds using an orbital shaker. Donor (460 nm) and acceptor (618 nm) emissions were measured within 10 minutes of substrate addition using the Envision microplate reader (Perkin Elmer) containing a 460/50 nm emission filter and a 610 nm LP filter. The BRET signal was calculated using the following formula: acceptor 618 nm emission/donor 460 nm emissions × 1,000.

For saturation curve analysis, a 6-point saturation curve was generated in which cells plated in a 6-well dish were transfected with a constant amount (5 ng) of the energy donor construct (Nano-CRAF) and increasing amounts (0–100 ng) of the energy acceptor plasmid (Halo-KRAS). For competition experiments, a non-BRET-tagged construct encoding the CRAF regulatory domain (pcDNA3-FLAG-CRAF-Reg) was co-transfected into cells at increasing DNA concentrations along with the Nano-$CRAF^{WT}$ (5 ng) and Halo-$KRAS^{Q61R}$ (25 ng) constructs. Following transfection, cells were processed, and BRET signals determined as described above.

Data analysis

The donor emission value, acceptor emission value, and the BRET signal were normalized for each test sample based on the averaged values obtained from wells on each plate that were treated with DMSO alone. Z′ values were calculated using methods described in ref. 13. IC_{50} values were estimated from dose–response curves using Prism (GraphPad) or SigmaPlot (SPSS Inc.) 4-parameter logistic nonlinear regression analysis. *P* values presented in the Results section are derived from Student *t* tests (unpaired, two sided, assuming unequal variance; GraphPad Prism). Significant values are indicated in figures (*, $P < 0.05$; **, $P < 0.01$; ***, $P < 0.001$; and ****, $P < 0.0001$).

Recombinant lentivirus and stable cell line generation

Recombinant lentivirus particles were generated by co-transfecting psPAX2 and pMD2 with the pLenti Halo-$KRAS^{G12V}$ construct into 293T cells using the X-tremeGENE9 transfection reagent. A total of 72 hours after transfection, the virus-containing supernatant was collected, centrifuged to remove any cellular debris, and then stored at −80°C. MCF10A cells were infected with viral supernatants containing 8 μg/mL polybrene for 24 hours, following which growth media containing 0.8 μg/mL puromycin was added.

Cell lysis, immunoprecipitation, and analysis of cell signaling

Cells were washed twice with ice cold PBS and lysed in NP-40 lysis buffer [20 mmol/L Tris (pH 8.0), 137 mmol/L NaCl, 10% glycerol, 1% NP-40 alternative, 0.15 U/mL aprotinin, 1 mmol/L phenylmethylsulfonyl fluoride, 0.5 mmol/L sodium vanadate, 20 μmol/L leupeptin] for 15 minutes at 4°C on a rocking platform. Lysates were collected and clarified by centrifugation at 14,000 rpm for 10 minutes at 4°C, following which protein content was determined by Bradford assays. Lysates containing equivalent amounts of protein were incubated with the appropriate antibody and protein G Sepharose beads for 2 hours at 4°C on a rocking platform. The immune complexes were collected, washed extensively with NP-40 lysis buffer, and examined by immunoblot analysis along with aliquots of total cell lysate. For signaling studies, the indicated cell lines were plated at approximately 70% confluency. A total of 48 hours after plating, cells were treated as indicated with the appropriate compound and then lysed. Lysates were equalized for protein content and examined by immunoblot analysis.

Surface plasmon resonance binding

Surface plasmon resonance (SPR) binding experiments were performed on a Biacore S200 instrument (GE Healthcare). Avi-$KRAS^{G12D}$ (amino acids 2–188) loaded with the non-hydrolyzable GTP analog, GppNHp, or avi-tagged CRAF-RBD (amino acids 52–131) were captured on CM5 sensor chips (GE Healthcare) containing amine coupled Neutravidin (10,000 RU). For single dose binding, compounds were diluted to 100 μmol/L in buffer containing 20 mmol/L HEPES

(pH 7.5), 150 mmol/L NaCl, 0.05% Tween 20, 5 mmol/L $MgCl_2$, and 2.5% DMSO prior to injection over avi-CRAF-RBD (3,000 RU) or over avi-$KRAS^{G12D}$-GppNHp (3,800 RU). For dose–response binding, a 2-fold dilution series of each compound was prepared (100–1.56 μmol/L in the above buffer) and injected over avi-RAF-RBD (1,785 RU) or over avi-$KRAS^{G12D}$-GppNHp (2,300 RU). The data were processed by subtracting binding responses on the reference flow cells as well as binding responses when buffer was injected. The samples were also corrected for DMSO mismatches using a DMSO standard curve.

Results

Development and validation of a NanoBRET assay monitoring RAS/RAF binding in live cells

The BRET methodology was used for the development of our screening platform (14), as BRET allows for protein–protein interactions to be monitored in real time and in a live cell context. This assay involves the use of target proteins in which one target is tagged with an energy donor and the second is tagged with an energy acceptor. When the two target proteins interact, the donor and acceptor tags are brought in close proximity such that energy from the donor is transferred to the acceptor, resulting in acceptor fluorescence that is used to determine the BRET signal (acceptor emission/donor emission; **Fig. 1A**). For our screen, we chose to use the NanoBRET system, in which the NanoLuc (Nano)-tag serves as the energy donor and the Halo-tag functions as the energy acceptor (15). An advantage of this system is that NanoLuc is a smaller and more robust energy donor than those used in traditional BRET assays and in combination with the Halo-tag 618 TM ligand, provides a wide spectral separation of the donor and acceptor emission peaks, resulting in a broad dynamic range.

Mutant KRAS and full-length, wild-type (WT) CRAF were selected as the BRET pair, given that KRAS is the RAS family member most frequently mutated in human cancer (3) and that our previous BRET analysis revealed that mutant KRAS produces the strongest BRET signal when paired with CRAF (11). In addition, because a primary objective of the screen would be to identify compounds that reduce signal output, the Q61R mutant of KRAS was utilized as the energy acceptor due to its high GTP occupancy (16) and ability to generate a higher BRET signal across a range of acceptor to donor ratios than did the G12D or G12V mutants (**Fig. 1B**). Moreover, based on saturation curve analysis and donor titration studies, an acceptor to donor ratio of 5 was used for further assay validation and screening, as this ratio yielded a strong BRET signal and lay within the ideal dynamic range for detecting changes in RAS/RAF binding (**Fig. 1C** and **D**).

To confirm the specificity of the NanoBRET assay, proteins containing mutations known to alter the RAS/RAF interaction were first analyzed. As shown in **Fig. 1E**, when the RBD of Nano-CRAF contained the R89L mutation that disrupts RAS binding, the BRET signal was reduced > 94% in comparison with that generated by the Halo-$KRAS^{Q61R}$/Nano-$CRAF^{WT}$ pair. Likewise, a significant reduction in the BRET signal (∼80%) was observed when the farnesylation and membrane binding of Halo-$KRAS^{Q61R}$ was disrupted by the C185A mutation (**Fig. 1E**). The effect of these mutations on RAS/RAF binding were further confirmed in co-immunoprecipitation assays (**Fig. 1F**).

Next, to demonstrate that binding between Halo-$KRAS^{Q61R}$ and Nano-$CRAF^{WT}$ could be disrupted in live cells, we employed a competition-based approach in which a non-BRET-tagged protein encoding the CRAF regulatory domain (CRAF-Reg, which contains the RBD) was coexpressed with the Halo-$KRAS^{Q61R}$/Nano-$CRAF^{WT}$ pair. As shown in **Fig. 2A**, CRAF-Reg was able to inhibit the interaction of full-length Nano-$CRAF^{WT}$ and Halo-$KRAS^{Q61R}$ in a dose-dependent manner, achieving an 82% reduction in the BRET signal.

Because there are no known inhibitors that can directly block the RAS/RAF interaction, further assay validation was conducted using compounds that indirectly alter this interaction. For example, ERK-mediated feedback phosphorylation of the RAFs is part of a well-established regulatory circuit to disrupt RAS/RAF binding and attenuate RAS signaling (17). As a result, when oncogenic RAS delivers a persistent signal, the RAFs must be continually dephosphorylated to restore their RAS-binding capability. Therefore, when cells were treated with the phosphatase inhibitor okadaic acid, a significant reduction in the BRET signal (∼40% to 60%) was observed that correlated with the accumulation of hyperphosphorylated, RAS-binding incompetent Nano-$CRAF^{WT}$ (**Fig. 2B**).

Next, we evaluated the effect of treating cells with the farnesyl transferase inhibitor FTI227. As expected, given the compensatory mechanism whereby KRAS can be geranylgeranylated to restore plasma membrane binding, FTI227 treatment for either 24 or 48 hours did not decrease the Halo-$KRAS^{Q61R}$/Nano-$CRAF^{WT}$ interaction (**Fig. 2C**). In contrast, cells expressing Halo-$HRAS^{Q61R}$ and Nano-$CRAF^{WT}$ exhibited a time-dependent reduction in the BRET signal (**Fig. 2C**). These findings are consistent with the selective displacement of Halo-HRAS, but not Halo-KRAS, from the plasma membrane by FTI treatment and demonstrate the specificity of the assay and its ability to detect compounds that target specific RAS/RAF complexes.

Finally, to determine whether the NanoBRET assay can also be used to identify compounds that augment the RAS/RAF interaction, we examined the effect of treating cells with the RAF inhibitor SB590885. Although ATP-competitive RAF inhibitors are well known for their ability to promote and stabilize RAF dimers, binding of these compounds to the RAF catalytic domain has also been reported to disrupt RAF autoinhibition and, in turn, facilitate RAS binding (18). Consistent with this report, when cells were treated with the RAF inhibitor SB590885, the interaction between Halo-$KRAS^{Q61R}$ and Nano-$CRAF^{WT}$ was increased approximately 35% (**Fig. 2D**). Thus, taken together, the above results demonstrate the effectiveness of the NanoBRET assay in detecting compounds that can modulate $KRAS^{Q61R}$/$CRAF^{WT}$ binding.

Optimization of the RAS/RAF NanoBRET assay for high-throughput screening

To maximize the efficiency and sensitivity of the NanoBRET assay for screening purposes, further studies were conducted to determine the optimal cell plating density, conditions for compound treatment, as well as the repeatability of the assay. With regard to plating densities, we found that the donor emission was linear with respect to cell number when cells were plated at densities of 4,000 to 8,000 cells per well, but not when plated at a higher cell density of 12,000 cells per well (**Fig. 3A**). Nonetheless, because the ratiometric format of the assay readout (acceptor 618 nm emission/donor 460 nm emission) insulates against variations in cell number, only a small decrease in the BRET signal was observed at the higher cell density (**Fig. 3A**), demonstrating a broad effective window. The assay was further found to have a Z'-factor of 0.6 and a signal to background ratio of >17, indicating a high-quality assay well suited for high-throughput screening (HTS) and one insensitive to small variations in cell number.

A test set of 352 natural product extracts was next used to evaluate various sample incubation times and to confirm the suitability of the assay for natural products discovery. When incubation periods of 1, 2, and 4 hours were compared, detection of inhibitory compounds

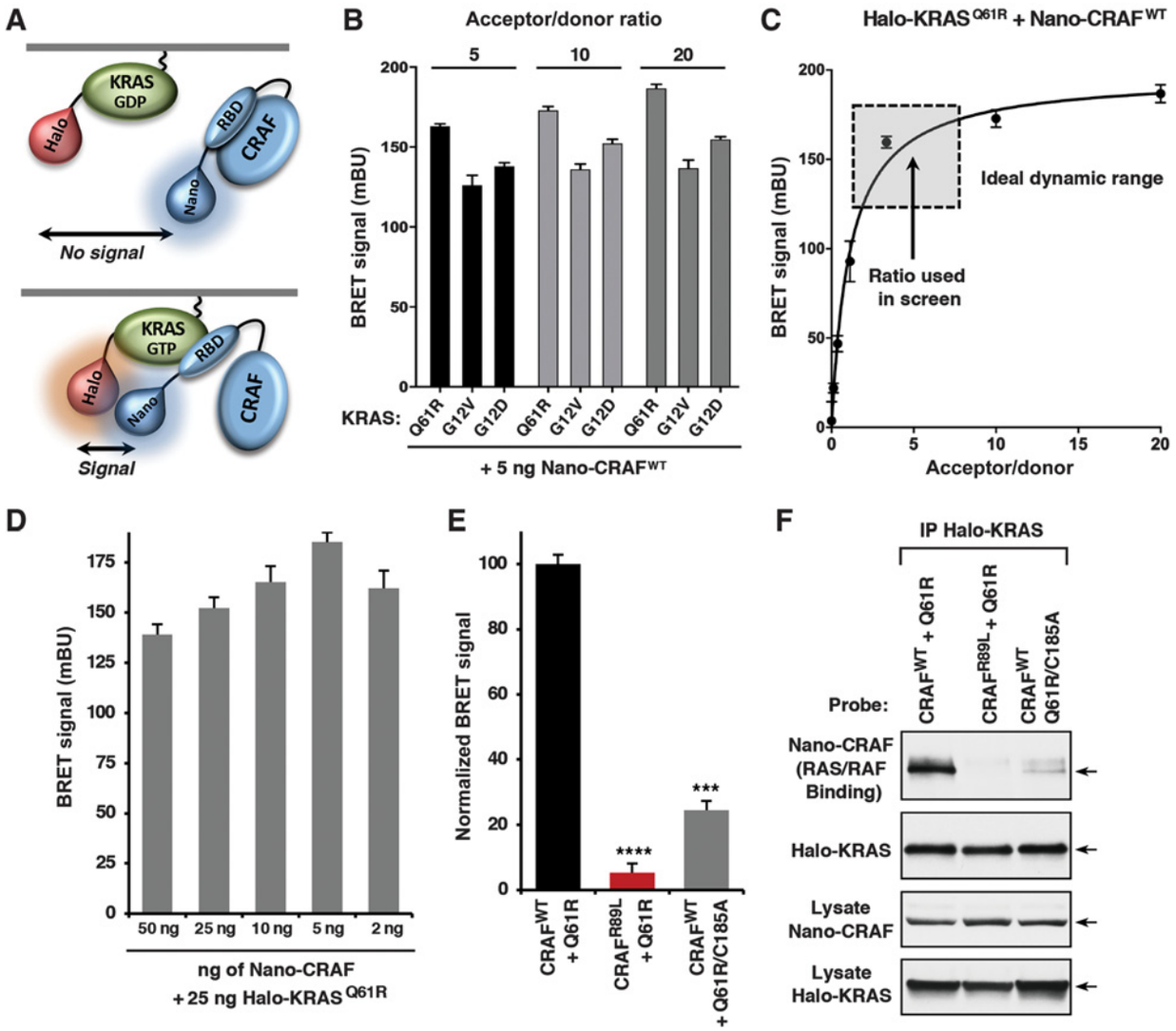

Figure 1.

Development and validation of the NanoBRET RAS/RAF interaction assay. **A,** Model illustrating the proximity-based NanoBRET assay. **B,** Comparison of the BRET signals obtained when 5 ng of the Nano-CRAF^{WT} donor construct was co-transfected with Halo-KRAS Q61R, G12V, or G12D acceptor constructs at acceptor to donor ratios of 5 (25 ng), 10 (50 ng), or 20 (100 ng). **C,** Shown is a NanoBRET saturation curve in which increasing amounts of the Halo-KRAS^{Q61R} acceptor construct were co-transfected with 5 ng of the Nano-CRAF^{WT} donor construct. The gray box indicates the ideal dynamic range for HTS and the black arrow signifies the 5:1 acceptor to donor ratio used in this screen. **D,** Nano-CRAF^{WT} was titrated from 50 to 2 ng of transfected plasmid DNA to obtain the highest BRET ratio when paired with 25 ng of Halo-KRAS^{Q61R}. **E,** Comparison of the BRET signal generated by the binding competent KRAS^{Q61R} and CRAF^{WT} NanoBRET pair (used for normalization) with BRET signals generated when the CRAF^{R89L} mutant that fails to bind RAS was used as the energy donor and when the KRAS$^{Q61R/C185A}$ mutant that is unable to localize to the plasma membrane was used as the energy acceptor. **F,** Lysates were prepared from 293FT cells expressing the BRET pairs KRAS^{Q61R}/CRAF^{WT}, KRAS^{Q61R}/CRAF^{R89L}, or KRAS$^{Q61R/C185A}$/CRAF^{WT}. Halo-KRAS^{Q61R} proteins were immunoprecipitated from the lysates and probed for the presence of Nano-CRAF and Halo-KRAS proteins. Total cell lysates were also examined for the expression of the BRET-tagged proteins. Blots are representative of three independent experiments with similar results. **B–E,** Data points represent BRET signals of quadruplicate wells from at least two independent experiments, with mean ± SD. ***, $P < 0.001$; ****, $P < 0.0001$.

improved with increased time (**Fig. 3B**, left). However, when sample incubation was expanded to 18 hours, high data scatter was observed, likely reflecting increased cellular toxicity (**Fig. 3B**, right). In addition, the BRET signal was unaffected by DMSO concentration up to 1% (**Fig. 3C**), a concentration above that needed for sample delivery. Therefore, based on the above findings, all subsequent assays were performed using 4,000 cells per well with a 4-hour sample incubation time.

Finally, compounds in the LOPAC library as well as the test series of natural product extracts were used to determine the day-to-day repeatability of the assay. As indicated in **Fig. 3D**, an excellent correlation was observed when the results of cells treated with the identical compounds on two separate days were plotted against one another. Further comparison revealed that the average multiple read variation of individual samples ranged from 5% to 8% over 9 repeats, confirming that the assay was highly reproducible.

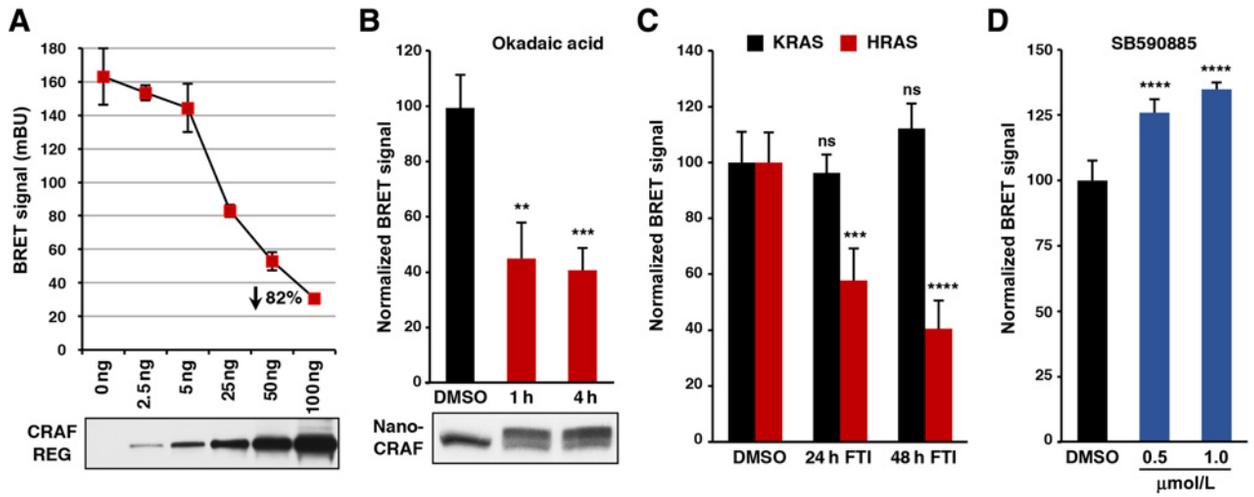

Figure 2.

The NanoBRET assay detects positive and negative modulators of RAS/RAF binding. **A,** 293FT cells were transfected with constructs expressing the NanoBRET pair, Halo-KRAS^{Q61R} and Nano-CRAF^{WT}, together with increasing amounts of a non-BRET-tagged CRAF regulatory domain construct (CRAF-REG). 48 hours after transfection, the BRET signal was determined, and cells were monitored for the increased expression of CRAF-REG. **B,** 293FT cells expressing Halo-KRAS^{Q61R}/Nano-CRAF^{WT} were treated with the phosphatase inhibitor okadaic acid (0.5 µmol/L) for 1 or 4 hours. BRET signals were then determined and normalized to the signal obtained from cells treated with DMSO. Cells were also evaluated for the hyperphosphorylation and reduced electrophoretic mobility of Nano-CRAF^{WT}. **C,** 293FT cells expressing Nano-CRAF^{WT} and either Halo-KRAS^{Q61R} or Halo-HRAS^{Q61R} were treated with the farnesyl transferase inhibitor, FTI227 (10 µmol/L), for 24 or 48 hours to block RAS farnesylation, following which normalized BRET signals were determined. **D,** Cells expressing Halo-KRAS^{Q61R}/Nano-CRAF^{WT} were treated with the RAF inhibitor SB590885 at concentrations of 0.5 and 1 µmol/L for 4 hours prior to determining the normalized BRET signals. Data (**A–D**) represent BRET signals of quadruplicate wells from at least two independent experiments, with mean ± SD. ns, not significant; **, $P < 0.01$; ***, $P < 0.001$, and ****, $P < 0.0001$.

Application to HTS

Using the optimized RAS/RAF NanoBRET assay, various libraries containing synthetic compounds, targeted inhibitors, purified natural products, and natural product extracts were evaluated. A summary of the samples screened and the criteria by which active (i.e., "hit") compounds were identified and confirmed is shown in Supplementary Table S2. Across 884 plates screened, the average variation of the control BRET ratio was 7.0% and, based on statistical evaluation of the screening data required to give >3 SDs from control, primary inhibitor hits were defined as those reducing the BRET output to less than 60% of control (summarized in Supplementary Table S3). To eliminate hits that impact the BRET signal due to toxicity issues, effects on the donor luciferase readout were evaluated and any compound that reduced the donor emission greater than 50% were excluded, as were compounds that increased donor emission greater than 150%. In addition, a small number of hits were also eliminated on the basis of color and/or intrinsic fluorescence that interfered with the donor or acceptor emissions (Supplementary Fig. S1). Active samples were confirmed in quadruplicate at the screening concentration, and dose–response curves were performed to obtain an estimate of potency.

On the basis of the hit criterion described, the screen resulted in the identification of numerous pure compounds that reproducibly inhibited the KRAS^{Q61R}/CRAF^{WT} interaction (hereon referred to as inhibitor compounds; **Table 1**). In addition, 99 natural product extracts, originating from plant, fungal, and animal sources, were also identified as inhibitor hits and will be evaluated at a later date upon purification and chemical characterization of the active components. Although the primary goal of the screening effort was to identify inhibitors of RAS/RAF binding, the screen also identified several compounds that enhanced the KRAS^{Q61R}/CRAF^{WT} interaction (defined as increasing the BRET signal >30%; Supplementary Table S4). Not surprising, most of the enhancer compounds were known RAF inhibitors or other ATP-competitive kinase inhibitors that may have off-target activity toward RAF.

Further characterization of inhibitor compounds

A subset of 20 inhibitor compounds were selected for analysis by SPR to determine whether any exhibited direct binding to activated KRAS or the CRAF-RBD (**Table 1**). Of note, the determination of this subset was based on the quantity of the compound available, its efficacy in reducing the BRET signal, and its reported target/activity or lack thereof. From this analysis, we found that none of the compounds demonstrated high-affinity, specific binding to either KRAS^{G12D} or the CRAF-RBD (**Table 1**). However, the calmodulin inhibitor calmidazolium chloride did display non-selective and non-saturable binding to both KRAS^{G12D} and CRAF-RBD, the cyclic depsipeptide swinhopeptolide (19) showed slow on/off rates and possible non-specific binding to KRAS^{G12D} and CRAF-RBD, and the CMLD7877 compound exhibited binding to the CRAF-RBD at high concentrations (Supplementary Fig. S2). Thus, it is likely that a majority of the inhibitors may exert their effects through indirect mechanisms. On the basis of the reported targets and activities of the inhibitor hits, these compounds could be grouped into various categories, including those that bind calmodulin and/or impact Ca^{2+} signaling, ones that promote reactive oxygen species (ROS) generation or endoplasmic reticulum (ER) stress, some that interact with HSP90 chaperones, ones that alter plasma membrane function, and some of other/or unknown functions. Interestingly, the majority of the inhibitor hits were compounds derived from natural products, which remains a rich source of medicinal drugs (20, 21).

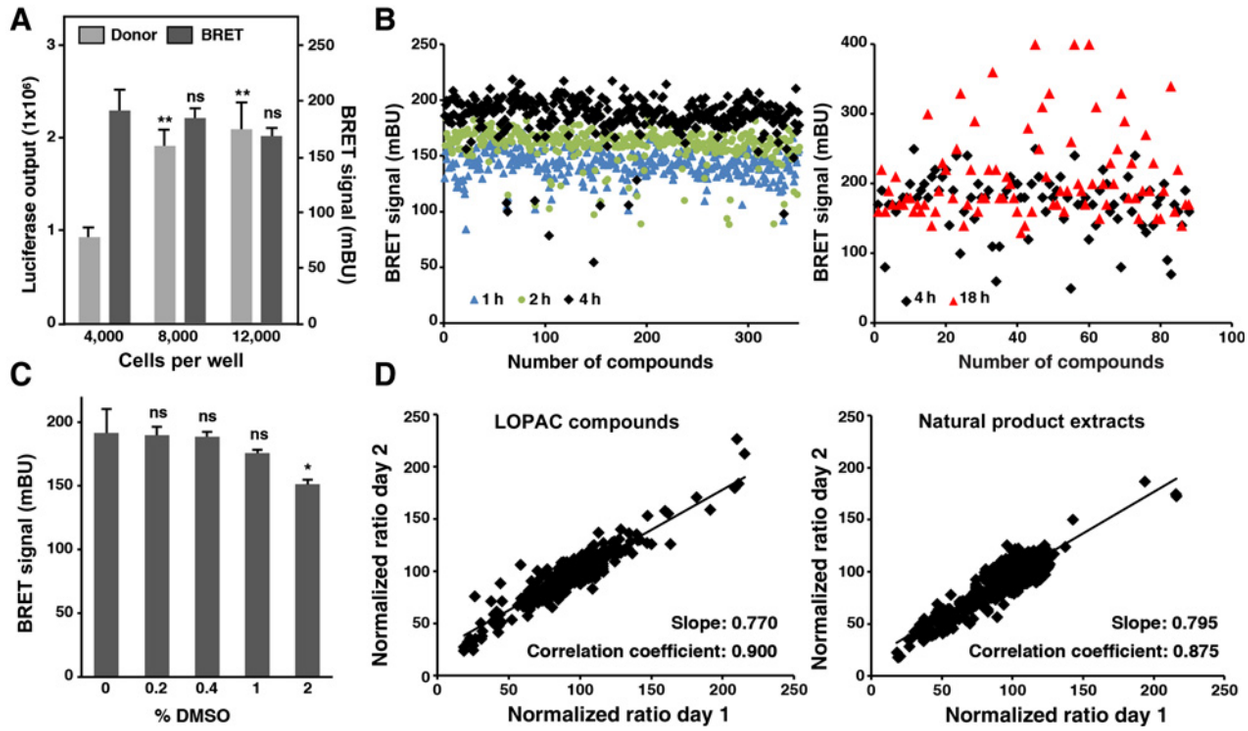

Figure 3.

Optimization of the NanoBRET RAS/RAF interaction assay for HTS. **A,** Cells expressing Halo-KRAS^{Q61R}/Nano-CRAF^{WT} were plated at densities of 4,000, 8,000, and 12,000 cells per well in a 384-well plate. The following day, donor emissions (luciferase output, light gray) and BRET signals (acceptor emission/donor emission) were determined (dark gray). Data represent quadruplicate wells from at least two independent experiments, with mean ± SD. ns, not significant; **, $P < 0.01$. **B,** Cells expressing the Halo-KRAS^{Q61R}/Nano-CRAF^{WT} BRET pair were plated at densities of 4,000 cells per well in a 384-well plate. The following day, cells were incubated with a test set of natural product extracts for 1, 2, or 4 hours, after which BRET signals (left) were determined. The effects of a 4- and 18-hour incubation period on the BRET signals were also compared (right). **C,** Cells expressing the Halo-KRAS^{Q61R}/Nano-CRAF^{WT} BRET pair were treated with increasing percentages of DMSO for 4 hours, prior to determining the BRET signal. Data are represented as the mean ± SD. ns, not significant; *, $P < 0.05$. **D,** Cells expressing the Halo-KRAS^{Q61R}/Nano-CRAF^{WT} BRET pair were plated at densities of 4,000 cells per well in a 384-well plate. The next day, cells were treated for 4 hours with either LOPAC samples (10 μmol/L) or a test set of natural product extracts and BRET signals were determined. From experiments conducted on two separate days, the BRET signals of each well on the day 1 (*x* axis) and day 2 (*y* axis) plates were plotted against each other to assess day-to-day repeatability. For the LOPAC samples, the slope was 0.770, with a correlation coefficient of 0.900 and for the natural product extracts, the slope was 0.798, with a correlation coefficient of 0.875. Average difference between the two reads was 5.1%–7.6%.

Signaling effects of modulating the RAS/RAF interaction

Experiments were next conducted to confirm that the NanoBRET screen not only identified compounds that modulate KRAS/CRAF binding, but also the signaling pathway that functions downstream of this interaction. For this analysis, we first evaluated one of the most potent inhibitors identified in the screen, ophiobolin A. Of note, ophiobolin A has been previously identified in a screen for compounds that disrupt the membrane organization of activated RAS proteins, where ophiobolin was reported to bind calmodulin and selectively inhibit the calmodulin-supported membrane nanoclustering of activated KRAS4B^{G12V} (22). For our signaling experiments, we used MCF10A epithelial cells that stably express Halo-KRAS^{G12V} as opposed to cancer cell lines expressing an activated KRAS allele, given that the mutational complexity characteristic of cancer lines can cause pathway feedback and cross-talk that could obscure the detection of signaling effects. As shown in **Fig. 4A**, treatment of these cells with ophiobolin A resulted in a dose-dependent decrease in the phosphorylation and activation of MEK and ERK (as monitored by pMEK and pERK levels), which correlated with the potency observed in the NanoBRET assay. Consistent with the work of Najumudeen and colleagues (22), we also found that ophiobolin A possessed significantly more activity than did the closely related ophiobolin C (Supplementary Fig. S3).

To demonstrate that the signaling effects were indeed RAS specific, we utilized RAS-deficient MEFs (4) that had been reconstituted to express either KRAS^{Q61R} or BRAF^{V600E}. In the KRAS^{Q61R} MEFs, ERK activation is dependent on RAS/RAF binding; however, in the BRAF^{V600E} MEFs, it is not, because these cells lack all RAS proteins and BRAF^{V600E} can signal to MEK as a RAS-independent monomer (23). Thus, compounds that inhibit signaling in a RAS-dependent manner would only be expected to decrease ERK activation in MEFs reconstituted with KRAS^{Q61R}. Consistent with this model, ophiobolin A treatment reduced pERK levels in a dose-dependent manner in the KRAS^{Q61R} MEFs, but not in the BRAF ^{V600E} MEFs (**Fig. 4B**). Further confirming the "in cell" disruption of the RAS/RAF interaction, ophiobolin A treatment of both MCF10A and MEF cells expressing mutant KRAS reduced the phosphorylation of CRAF on S338, an activating phosphorylation event that is RAS dependent and occurs at the plasma membrane (**Fig. 4C**; ref. 24).

Subsequent studies using these cell systems revealed that another potent inhibitor, gliotoxin, as well as the CMLD 7877 compound, which displayed binding to the CRAF-RBD at high concentrations

Table 1. Compounds identified as inhibitors of the $KRAS^{Q61R}$/$CRAF^{WT}$ interaction.

Inhibitor compounds	IC_{50} μmol/L (95% CI)[a]	Putative target/activity(s)	Reference
Calmidazolium chloride[b]	3.6 (3.3–3.9)	Calmodulin inhibitor	(32)
Trifluoperazine	14.3 (12.8–16.0)	Calmodulin inhibitor, dopamine receptor antagonist	(33, 34)
Ophiobolin A[c] (NP)	1.08 (0.59–1.39)	Calmodulin inhibitor, alters KRAS nanoclusters, ER stress	(22, 35)
Striatin E (NP)	6.3 (5.2–8.3)	Calmodulin binding, alters IKK β, JAK-STAT, MAPK signaling	(36, 37)
Gossypol (NP)	5.2 (4.6–5.8)	Dehydrogenase inhibitor, calmodulin binding	(38, 39)
A23187[c] (NP)	0.85 (0.71–1.0)	Calcium ionophore	(40)
NNC 55–0396[c]	7.1 (6.5–7.8)	T-type calcium channel inhibitor	(41)
Thapsigargin (NP)	14.0 (12.7–15.7)	SR Ca^{2+}-ATPase inhibitor, ER stress/ROS	(42)
Terfenadine	6.0 (5.5–6.5)	Histamine receptor H1 inhibitor, Ca^{2+}, ROS, hERG channel inhibitor	(43–45)
Callipeltin A[c] (NP)	1.1 (0.7–1.5)	Na^{+}/Ca^{2+} exchange inhibitor	(46)
Chetomin (NP)	2.9 (2.1–3.8)	Induces ROS/ER stress and Ca^{2+} influx, thiol reactive, HIF1 inhibitor	(47, 48)
Gliotoxin[c] (NP)	2.8 (1.3–3.8)	ROS inducer, thiol reactive	(49)
Scabrosin diacetate (NP)	3.4 (2.7–4.1)	ROS inducer, thiol reactive, inhibits mitochondrial ATP synthase	(50)
Varacin (NP)	9.5 (7.5–12.5)	ROS inducer	(51)
Gambogic acid (NP)	1.7 (1.3–2.1)	HSP90β inhibitor, affects multiple signaling pathways	(26, 52)
NSC145366[c]	5.2 (4.7–5.7)	Allosteric HSP90 inhibitor (binds HSP90 CTD)	(53)
Polyphyllin B (diosgenin tetraglycoside, formosanin C, Paris saponin II)[c] (NP)	3.3 (2.9–3.7)	Saponin, mitochondrial effects, IKK β inhibition	(54)
Elliptoside J (NP)	9.8 (8.5–13.8)	Saponin, membrane-reactive	(55)
Ardisiacrispin A (NP)	3.8 (3.2–4.3)	Saponin, membrane-reactive	(56, 57)
Ardisiacrispin B (NP)	5.0 (4.4–5.8)	Saponin, membrane-reactive	(56, 57)
Cyclaminorin (NP)	4.2 (3.7–5.0)	Saponin, membrane-reactive	(56, 57)
3-O-a-L-Rhamnopyranosyl-(1–2)-ß-D-glucopyranosyl-(1–4)-a-L-arabinopyranosylcyclamiretin A (NP)	3.7 (3.3–4.3)	Saponin, membrane-reactive	(56, 57)
NSC164914[c]	3.5 (3.0–4.1)	Aquaporin inhibitor	(58)
Bromoacetyl alprenolol methane	6.5 (6.0–7.0)	β-AR antagonist, neddylation inhibitor	(59, 60)
Candesartan cilexetil	5.4 (4.6–6.7)	Angiotensin receptor antagonist	(61)
L703–606	7.0 (6.3–7.8)	NK1 neurokinin receptor antagonist	(62)
MK886	7.7 (7.1–8.1)	Leukotriene antagonist	(63)
NSC33353[c]	5.9 (5.2–6.6)	AcrA inhibitor	(64)
NSC620358 (NP)	16.2 (13.2–21.0)	Ubiquitin-proteosome inhibitor	(65)
Isolissochlinotoxin B[c] (NP)	5.5 (4.0–8.1)	HDM2 ubiquitin ligase	(66)
Ugandensidial[c] (NP)	~8.7	12(S)-HETE, leukotriene B biosynthesis	(67)
Malformin B (NP)	7.2 (5.9–8.4)	Unknown	(68)
NP-006581[c] (NP)	~10	Unknown	
Swinhopeptolide[b] (NP)	3.6 (3.3–3.9)	Unknown	(19)
13-epi-9-deacetoxyxenicin[c] (NP)	2.6 (0.8–3.2)	Unknown	(69)
Aciculitin B[c] (NP)	4.0 (3.2–6.1)	Unknown	(70)
CMLD5181[b]	5.4 (5.2–5.6)	Unknown	na
CMLD7873[b]	9.4 (7.8–19.6)	Unknown	na
CMLD7877[b]	4.32 (3.95–4.69)	Unknown	na
CMLD7896[b]	5.3 (<5.9)[d]	Unknown	na
CMLD7898[b]	6.6 (<7.6)[d]	Unknown	na

[a]NanoBRET IC_{50} and 95% confidence interval calculated from 4-parameter logistic curve fitting.
[b]Tested in SPR analysis and showed no binding to $KRAS^{G12V}$ or CRAF-RBD.
[c]Tested in SPR analysis and exhibited binding to $KRAS^{G12V}$ or CRAF-RBD that was likely nonspecific or only observed at high concentrations. (NP) designates compounds that are derived from natural products.
[d]Lower limit of confidence interval could not be calculated.

in the SPR analysis, could also inhibit RAS-dependent ERK activation (**Fig. 5A** and **B**). With regard to gliotoxin, it is a drug known to induce ROS generation, and like rigosertib and paclitaxel, two cancer therapies that promote ROS generation through effects on microtubules, it is likely that gliotoxin treatment activates a stress-induced phosphoregulatory circuit that leads to the hyperphosphorylation of CRAF on sites that prevent RAS binding (25).

Next, we examined the signaling effects of an inhibitor compound whose activity would be predicted to be RAF-dependent, NSC145366. NSC145366 is a reported allosteric inhibitor of HSP90, and the RAF kinases require HSP90 activity for proper protein folding and stability. As shown in **Fig. 5C** and **D**, NSC145366 treatment not only inhibited ERK activation in cells expressing mutant KRAS, it also suppressed pERK levels in the $BRAF^{V600E}$

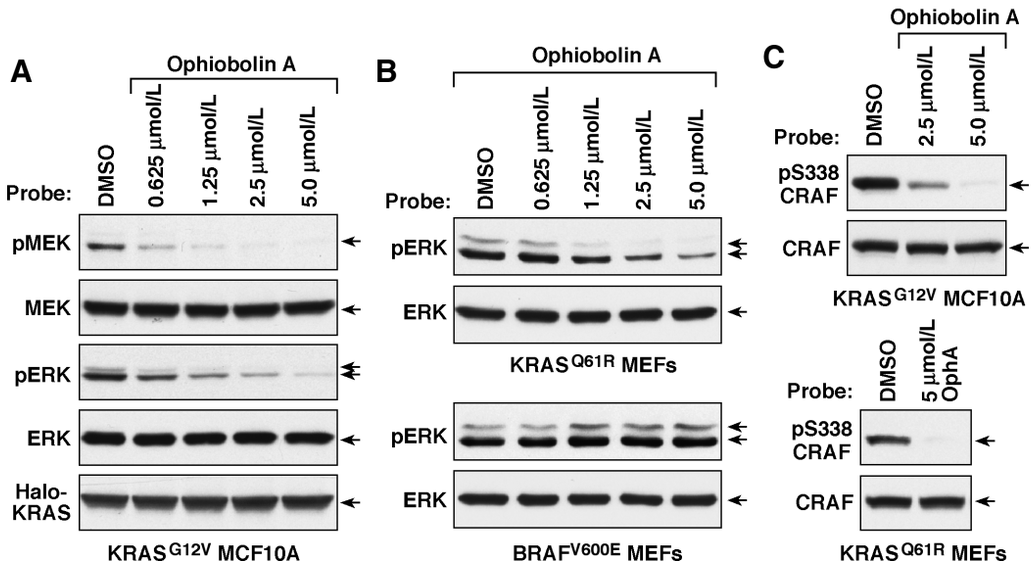

Figure 4.

Effects of the inhibitor compound ophiobolin A on cell signaling. **A,** MCF10A cells stably expressing Halo-KRAS^{G12V} were treated with the indicated concentration of ophiobolin A for 1 hour prior to lysis. Lysates were then examined for pMEK and pERK levels as well as for total MEK, ERK, and Halo-KRAS^{G12V} levels. **B,** RAS-deficient MEFs reconstituted with KRAS^{Q61R} or BRAF^{V600E} were treated with the indicated concentration of ophiobolin A for 1 hour prior to lysis. Lysates were then examined for pERK and total ERK levels. **C,** KRAS^{G12V}-MCF10 A cells (top) or reconstituted KRAS^{Q61R} MEFs (bottom) were treated with the indicated concentration of ophiobolin A for 1 hour prior to lysis. Lysates were then examined for the phosphorylation of endogenous CRAF on S338 (pS338-CRAF) and for total CRAF levels. Blots are representative of at least two independent experiments with similar results.

MEFs, consistent with the requirement for HSP90 in BRAF^{V600E} function.

Finally, we evaluated a compound identified as an "enhancer" hit, AG825, which is a reported ATP-competitive tyrosine kinase inhibitor. As expected for a compound that facilitates RAS/RAF binding, treatment with AG825 increased RAS-dependent ERK activation in cells expressing mutant KRAS. However, in MEFs reconstituted with BRAF^{V600E}, pERK levels were reduced to a level similar to that observed when cells were treated with the known RAF inhibitor SB590885 (**Fig. 5E** and **F**). In addition, AG825 was found to increase the detection of heterodimerized CRAF/BRAF complexes in KRAS^{Q61R}-MEFs, consistent with direct, off-target binding to the RAF kinase domains (**Fig. 5G**). Taken together, the above findings provide proof-of-principle that the RAS/RAF NanoBRET assay can, in an unbiased manner, identify functionally relevant modulators of the RAS/RAF interaction.

Discussion

Here, we describe the development and application of a screening platform that utilizes the NanoBRET methodology to detect compounds that can modulate the RAS/RAF interaction in live cells. The RAS GTPases are prominent drivers of human cancer, and for these proteins to exert their full oncogenic potential, they must interact with the RAF kinases to engage the ERK cascade and transmit proliferative signals. Therefore, the identification of compounds that can inhibit or disrupt RAS/RAF binding in a live cell environment may reveal new agents and/or strategies to counteract dysregulated RAS signaling in tumor cells.

Taking advantage of the NCI's diverse repertoire of screening libraries, including those containing small molecule inhibitors, known drug therapies, and purified natural products, a total of 74,735 pure compounds and 207,209 partially purified natural product extracts were evaluated for their effects on KRAS^{Q61R}/CRAF^{WT} binding. Through these efforts, both inhibitors and enhancers of this critical interaction were identified. A subset of the inhibitor hits from the pure compound libraries were subsequently analyzed by SPR for binding to active KRAS or the CRAF-RBD. Interestingly, none of the compounds were found to be direct competitors of the RAS/RAF interaction, suggesting that the majority of inhibitor hits mediate their effects through indirect mechanisms. On the basis of the targets and activities reported for these compounds, the inhibitor hits could be grouped into several categories, including some that would be predicted to impact RAS/RAF binding. These groups include modulators of calmodulin and/or Ca^{2+} signaling, inducers of ROS generation or ER stress, inhibitors of HSP90 chaperones, compounds that are thiol reactive, ones that alter plasma membrane function, and some of other/or unknown functions.

Strikingly, this is the second time that ophiobolin A, a known binder of calmodulin, has been identified in a screen for inhibitors of mutant KRAS function. Previously, ophiobolin A was found to disrupt the calmodulin-supported membrane nanoclustering of KRAS4B^{G12V} and here we find that it is a potent inhibitor of KRAS4B^{Q61R}/CRAF^{WT} binding and can suppress KRAS4B-dependent signaling. The inability to detect binding between ophiobolin A and KRAS or the CRAF RBD is also consistent with an indirect effect on RAS/RAF binding and downstream signal transduction. Interestingly, several other calmodulin-binding drugs (calmidazolium chloride, trifluoperazine, gossypol, and NSC312033) were scored as inhibitors of the KRAS4B^{Q61R}/CRAF^{WT} interaction, supporting a role for calmodulin in KRAS4B function. Moreover, several saponins (including polyphyllin B, ellipticoside J, ardisiacrispins, cyclaminorin), which can perturb biological membranes, were also identified as inhibitor hits, likely reflecting the importance of plasma membrane binding in KRAS signaling.

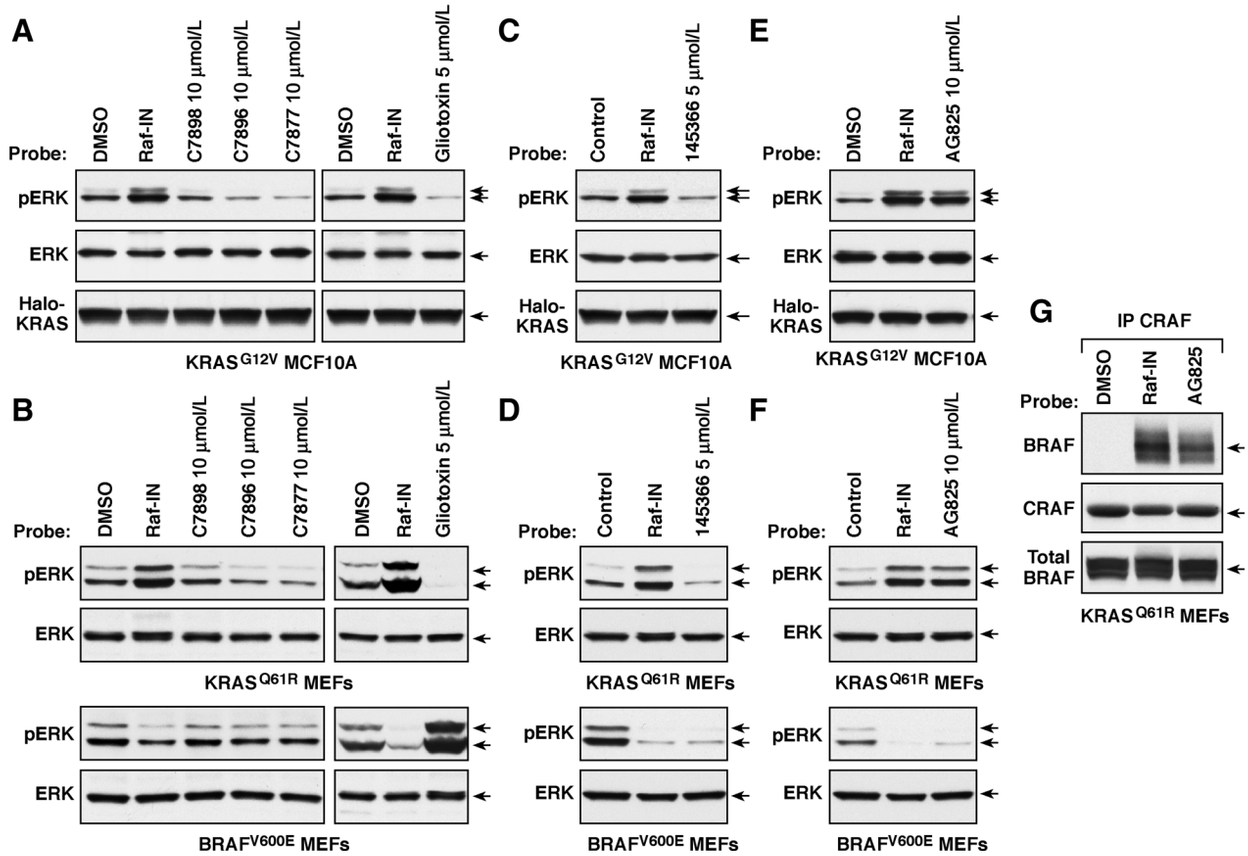

Figure 5.

Cell signaling effects of modulators of the RAS/RAF interaction. Analysis of compounds affecting RAS-dependent signaling: **A**, MCF10A cells stably expressing Halo-KRAS^{G12V} were treated with the indicated compounds for 1 hour prior to lysis. Treatment with DMSO and the RAF inhibitor SB590885 (1 μmol/L, RAF-IN) were used as controls. Lysates were then examined for pERK levels as well as for total ERK and Halo-KRAS^{G12V} levels. **B,** RAS-deficient MEFs reconstituted with KRAS^{Q61R} or BRAF^{V600E} were treated with the indicated compounds for 1 hour prior to lysis. Lysates were then examined for pERK and total ERK levels. Analysis of inhibitor compounds affecting RAF-dependent signaling: KRAS^{G12V}-MCF10A (**C**) cells were treated and analyzed as in **A**. KRAS^{Q61R} or BRAF^{V600E} MEFs (**D**) were treated and analyzed as in **B**. Effect of the AG825 enhancer compound on cell signaling: KRAS^{G12V}-MCF10A (**E**) cells were treated for 1 hour with either the RAF inhibitor SB590885 (1 μmol/L) or AG825 (10 μmol/L) prior to lysis. Lysates were examined for pERK, total ERK, and Halo-KRAS^{G12V} levels. **F,** KRAS^{Q61R} or BRAF^{V600E} MEFs were treated MEFs were treated as in **E**, and lysates were examined for pERK and total ERK levels. **G,** KRAS^{Q61R}-expressing MEFs were also examined for the effect of RAF inhibitor SB590885 or AG825 treatment on BRAF/CRAF dimer formation. Endogenous CRAF proteins were immunoprecipitated from lysates of cells treated with SB590885 (1 μmol/L) or AG825 (10 μmol/L) for 1 hour prior to lysis, and the isolated CRAF complexes were probed for the presence of BRAF and CRAF. The total BRAF level in lysates is also shown. Blots are representative of at least two independent experiments with similar results.

Inhibitor hits that may alter CRAF function include HSP90 inhibitors, compounds that induce ROS generation, as well as those that are thiol reactive. In particular, the RAF kinases are HSP90 client proteins and inhibiting the chaperone activity of HSP90 would be expected to disrupt the folding and functionality of the RAFs. Consistent with this model, the HSP90 inhibitor NSC145366 was found not only to reduce ERK activation mediated by KRAS^{Q61R} in reconstituted RAS-deficient MEFs but also that induced by BRAF^{V600E}. In addition, gambogic acid, an HSP90 inhibitor that selectively inhibits HSP90β (26), was also identified in our screen, a finding consistent with the identification of HSP90β peptides in RAF protein complexes by mass spectrometry (7).

Compounds that induce ROS or ER stress may act in a manner similar to rigosertib and paclitaxel, which engage a stress-induced phosphoregulatory circuit that results in the hyperphosphorylation of the RAFs on sites that impair RAS/RAF binding (25). Alternatively, ROS-inducing compounds that are members of the epidithiodioxopiperazine family and can form mixed disulfide bonds with free thiols (chetomin, gliotoxin, scabrosin diacetate), may also act by targeting zinc-binding proteins. For example, chetomin has been reported to disrupt the p300-HIF1 interaction by mediating the ejection of coordinated zinc ions from the CH1 domain of p300 (27). The RAF kinases also contain a zinc-binding, cysteine-rich domain (CRD) that stabilizes RAS/RAF/membrane interactions and is required to promote pathway activation (28, 29). Therefore, disrupting the RAF CRD structure could be another mechanism by which these compounds inhibit RAS/RAF binding. Indeed, the signaling effects observed for gliotoxin treatment would be consistent with this mechanism, given that ERK activation mediated by mutant KRAS would require RAF CRD function, but not that mediated by BRAF^{V600E}, as BRAF^{V600E} activity is not dependent on RAS or membrane binding. Of note, ophiobolin A is also a thiol-reactive compound and may exert its effects by altering the functions of both RAS and RAF.

With regard to the compounds that enhanced the RAS/RAF interaction, the majority were compounds known to be ATP-competitive kinase inhibitors, including four that directly target the RAF kinases and some that have off-target activity toward RAF (30). In agreement with the report by Jin and colleagues (18), we find that the NanoBRET assay is a very sensitive method for assessing the mode of inhibitor binding as the major determinant for the enhancing effect of these compounds was whether their binding placed the RAF αC-helix in the active position to disrupt RAF autoinhibition, thereby facilitating RAS binding (Supplementary Fig. S4).

In summary, the RAS/RAF NanoBRET assay has proven to be a very reproducible and effective assay for detecting agents that can modulate RAS/RAF binding in live cells. Its successful adaptation for HTS, further expands the possibility of identifying compounds that may have therapeutic potential in suppressing dysregulated RAS signaling. The variety of molecular targets and cellular activities reported for the inhibitor compounds identified in this screen suggests that many cellular factors can influence RAS/RAF binding and downstream signal transduction. Understanding the mechanisms by which these compounds exert their effects may reveal previously unknown regulatory events and pathway cross-talk that impact RAS or RAF function and may provide novel insights regarding the design of new combinatorial therapies with clinical benefit. Finally, the identification of a large number of pure natural products and active natural product extracts as inhibitors of the RAS/RAF interaction indicates that further drug discovery with natural products may be highly fruitful. Moreover, because polypharmacology is a common feature of natural products (31), compounds affecting multiple targets or pathways may be particularly advantageous for meaningful suppression of RAS-driven signaling.

Authors' Disclosures

No disclosures were reported.

Disclaimer

The content of this article does not necessarily reflect the views or policies of the Department of Health and Human Services, nor does mention of trade names, commercial products, or organizations imply endorsement by the U.S. Government.

Authors' Contributions

D.E. Durrant: Conceptualization, data curation, formal analysis, validation, investigation, visualization, methodology, writing–original draft, writing–review and editing. **E.A. Smith:** Formal analysis, investigation, visualization. **E.I. Goncharova:** Resources, data curation, formal analysis. **N. Sharma:** Formal analysis, investigation, visualization. **P.A. Alexander:** Validation, Investigation. **A.G. Stephen:** Data curation, validation, investigation, writing–review and editing. **C.J. Henrich:** Conceptualization, resources, data curation, formal analysis, supervision, funding acquisition, validation, investigation, visualization, methodology, writing–original draft, project administration, writing–review and editing. **D.K. Morrison:** Conceptualization, resources, data curation, formal analysis, supervision, funding acquisition, validation, investigation, visualization, methodology, writing–original draft, project administration, writing–review and editing.

Acknowledgments

The authors thank the NCI-RAS Initiative for providing critical reagents and John Beutler, Molecular Targets Program, for insights regarding various natural products. This project has been funded in whole or in part with federal funds from the NCI, NIH, under contract no. HHSN261200800001E. This research was also supported (in part) by the Intramural Research Program of the NIH, NCI, Center for Cancer Research under project numbers ZIA BC 010329 (D.K. Morrison) and ZIA BC 011469 (C.J. Henrich).

The costs of publication of this article were defrayed in part by the payment of page charges. This article must therefore be hereby marked *advertisement* in accordance with 18 U.S.C. Section 1734 solely to indicate this fact.

Received February 23, 2021; revised April 24, 2021; accepted June 15, 2021; published first June 22, 2021.

References

1. Cox AD, Der CJ. Ras history: the saga continues. Small GTPases 2010;1:2–27.
2. Bos JL, Rehmann H, Wittinghofer A. GEFs and GAPs: critical elements in the control of small G proteins. Cell 2007;129:865–77.
3. Prior IA, Lewis PD, Mattos C. A comprehensive survey of Ras mutations in cancer. Cancer Res 2012;72:2457–67.
4. Drosten M, Dhawahir A, Sum EY, Urosevic J, Lechuga CG, Esteban LM, et al. Genetic analysis of Ras signalling pathways in cell proliferation, migration and survival. EMBO J 2010;29:1091–104.
5. Simanshu DK, Nissley DV, McCormick F. RAS proteins and their regulators in human disease. Cell 2017;170:17–33.
6. Terrell EM, Morrison DK. Ras-mediated activation of the Raf family kinases. Cold Spring Harb Perspect Med 2019;9:a033746.
7. Freeman AK, Ritt DA, Morrison DK. Effects of Raf dimerization and its inhibition on normal and disease-associated Raf signaling. Mol Cell 2013;49:751–8.
8. Fabian JR, Vojtek AB, Cooper JA, Morrison DK. A single amino acid change in Raf-1 inhibits Ras binding and alters Raf-1 function. Proc Natl Acad Sci U S A 1994;91:5982–6.
9. Chung D, Amar S, Glozman A, Chen JM, Friedman FK, Robinson R, et al. Inhibition of oncogenic and activated wild-type ras-p21 protein-induced oocyte maturation by peptides from the ras-binding domain of the raf-p74 protein, identified from molecular dynamics calculations. J Protein Chem 1997;16:631–5.
10. Kimoto M, Shirouzu M, Mizutani S, Koide H, Kaziro Y, Hirao I, et al. Anti-(Raf-1) RNA aptamers that inhibit Ras-induced Raf-1 activation. Eur J Biochem 2002;269:697–704.
11. Terrell EM, Durrant DE, Ritt DA, Sealover NE, Sheffels E, Spencer-Smith R, et al. Distinct binding preferences between Ras and Raf family members and the impact on oncogenic Ras signaling. Mol Cell 2019;76:872–84.
12. Brown LE, Chih-Chien Cheng K, Wei WG, Yuan P, Dai P, Trilles R, et al. Discovery of new antimalarial chemotypes through chemical methodology and library development. Proc Natl Acad Sci U S A 2011;108:6775–80.
13. Zhang J, Chung T, Oldenburg K. A simple statistical parameter for use in evaluation and validation of high throughput screening assays. J Biomol Screen 1999;4:67–73.
14. Pfleger K, Eidne K. Illuminating insights into protein-protein interactions using bioluminescence resonance energy transfer (BRET). Nat Methods 2006;3:165–74.
15. Machleidt T, Woodroofe CC, Schwinn MK, Méndez J, Robers MB, Zimmerman K, et al. NanoBRET–a novel BRET platform for the analysis of protein-protein interactions. ACS Chem Biol 2015;10:1797–804.
16. Hunter JC, Manandhar A, Carrasco MA, Gurbani D, Gondi S, Westover KD. Biochemical and structural analysis of common cancer-associated KRAS mutations. Mol Cancer Res 2015;13:1325–35.
17. Dougherty MK, Müller J, Ritt DA, Zhou M, Zhou XZ, Copeland TD, et al. Regulation of Raf-1 by direct feedback phosphorylation. Mol Cell 2005;17:215–24.
18. Jin T, Lavoie H, Sahmi M, David M, Hilt C, Hammell A, et al. RAF inhibitors promote RAS-RAF interaction by allosterically disrupting RAF autoinhibition. Nat Commun 2017;8:1211.
19. Kim CK, Wang D, Bokesch HR, Fuller RW, Smith E, Henrich CJ, et al. Swinhopeptolides A and B: cyclic depsipeptides from the sponge Theonella swinhoei that inhibit Ras/Raf interaction. J Nat Prod 2020;83:1288–94.

20. Harvey AL, Edrada-Ebel R, Quinn RJ. The re-emergence of natural products for drug discovery in the genomics era. Nat Rev Drug Discov 2015;14:111–29.
21. Patridge E, Gareiss P, Kinch MS, Hoyer D. An analysis of FDA-approved drugs: natural products and their derivatives. Drug Discov Today 2016;21:204–7.
22. Najumudeen AK, Jaiswal A, Lectez B, Oetken-Lindholm C, Guzmán C, Siljamäki E, et al. Cancer stem cell drugs target K-ras signaling in a stemness context. Oncogene 2016;35:5248–62.
23. Poulikakos PI, Persaud Y, Janakiraman M, Kong X, Ng C, Moriceau G, et al. RAF inhibitor resistance is mediated by dimerization of aberrantly spliced BRAF (V600E). Nature 2011;480:387–90.
24. Mason CS, Springer CJ, Cooper RG, Superti-Furga G, Marshall CJ, Marais R. Serine and tyrosine phosphorylations cooperate in Raf-1, but not B-Raf activation. EMBO J 1999;18:2137–48.
25. Ritt DA, Abreu-Blanco MT, Bindu L, Durrant DE, Zhou M, Specht SI, et al. Inhibition of Ras/Raf/MEK/ERK pathway signaling by a stress-induced phospho-regulatory circuit. Mol Cell 2016;64:875–87.
26. Yim KH, Prince TL, Qu S, Bai F, Jennings PA, Onuchic JN, et al. Gambogic acid identifies an isoform-specific druggable pocket in the middle domain of Hsp90β. Proc Natl Acad Sci U S A 2016;113:E4801–9.
27. Cook KM, Hilton ST, Mecinovic J, Motherwell WB, Figg WD, Schofield CJ. Epidithiodiketopiperazines block the interaction between hypoxia-inducible factor-1alpha (HIF-1alpha) and p300 by a zinc ejection mechanism. J Biol Chem 2009;284:26831–8.
28. Bondeva T, Balla A, Varnai P, Balla T. Structural determinants of Ras-Raf interaction analyzed in live cells. Mol Biol Cell 2002;13:2323–33.
29. Roy S, Lane A, Yan J, McPherson R, Hancock JF. Activity of plasma membrane-recruited Raf-1 is regulated by Ras via the Raf zinc finger. J Biol Chem 1997;272:20139–45.
30. Lavoie H, Thevakumaran N, Gavory G, Li JJ, Padeganeh A, Guiral S, et al. Inhibitors that stabilize a closed RAF kinase domain conformation induce dimerization. Nat Chem Biol 2013;9:428–36.
31. Ho TT, Tran QT, Chai CL. The polypharmacology of natural products. Future Med Chem 2018;10:1361–8.
32. Gietzen K. Comparison of the calmodulin antagonists compound 48/80 and calmidazolium. Biochem J 1983;216:611–6.
33. Cook WJ, Walter LJ, Walter MR. Drug binding by calmodulin: crystal structure of a calmodulin-trifluoperazine complex. Biochemistry 1994;33:15259–65.
34. Chen Y, Luo F, Yang C, Kirkmire CM, Wang ZJ. Acute inhibition of Ca2+/calmodulin-dependent protein kinase II reverses experimental neuropathic pain in mice. J Pharmacol Exp Ther 2009;330:650–9.
35. Masi M, Dasari R, Evidente A, Mathieu V, Kornienko A. Chemistry and biology of ophiobolin A and its congeners. Bioorg Med Chem Lett 2019;29:859–69.
36. Gassner NC, Tamble CM, Bock JE, Cotton N, White KN, Tenney K, et al. Accelerating the discovery of biologically active small molecules using a high-throughput yeast halo assay. J Nat Prod 2007;70:383–90.
37. Petrova RD, Mahajna J, Reznick AZ, Wasser SP, Denchev CM, Nevo E. Fungal substances as modulators of NF-kappaB activation pathway. Mol Biol Rep 2007;34:145–54.
38. Benz CC, Keniry MA, Ford JM, Townsend AJ, Cox FW, Palayoor S, et al. Biochemical correlates of the antitumor and antimitochondrial properties of gossypol enantiomers. Mol Pharmacol 1990;37:840–7.
39. Carruthers NJ, Dowd MK, Stemmer PM. Gossypol inhibits calcineurin phosphatase activity at multiple sites. Eur J Pharmacol 2007;555:106–14.
40. Abbott BJ, Fukuda DS, Dorman DE, Occolowitz JL, Debono M, Farhner L. Microbial transformation of A23187, a divalent cation ionophore antibiotic. Antimicrob Agents Chemother 1979;16:808–12.
41. Huang L, Keyser BM, Tagmose TM, Hansen JB, Taylor JT, Zhuang H, et al. NNC 55–0396 [(1S, 2S)-2-(2-(N-[(3-benzimidazol-2-yl)propyl]-N-methylamino) ethyl)-6-fluoro-1,2,3,4-tetrahydro-1-isopropyl-2-naphtyl cyclopropanecarboxylate dihydrochloride]: a new selective inhibitor of T-type calcium channels. J Pharmacol Exp Ther 2004;309:193–9.
42. Linxweiler M, Schorr S, Schäuble N, Jung M, Linxweiler J, Langer F, et al. Targeting cell migration and the endoplasmic reticulum stress response with calmodulin antagonists: a clinically tested small molecule phenocopy of SEC62 gene silencing in human tumor cells. BMC Cancer 2013;13:574.
43. Hove-Madsen L, Llach A, Molina CE, Prat-Vidal C, Farré J, Roura S, et al. The proarrhythmic antihistaminic drug terfenadine increases spontaneous calcium release in human atrial myocytes. Eur J Pharmacol 2006;553:215–21.
44. Nicolau-Galmés F, Asumendi A, Alonso-Tejerina E, Pérez-Yarza G, Jangi SM, Gardeazabal J, et al. Terfenadine induces apoptosis and autophagy in melanoma cells through ROS-dependent and -independent mechanisms. Apoptosis 2011;16:1253–67.
45. Tanaka H, Takahashi Y, Hamaguchi S, Iida-Tanaka N, Oka T, Nishio M, et al. Effect of terfenadine and pentamidine on the HERG channel and its intracellular trafficking: combined analysis with automated voltage clamp and confocal microscopy. Biol Pharm Bull 2014;37:1826–30.
46. Trevisi L, Bova S, Cargnelli G, Danieli-Betto D, Floreani M, Germinario E, et al. Callipeltin A, a cyclic depsipeptide inhibitor of the cardiac sodium-calcium exchanger and positive inotropic agent. Biochem Biophys Res Commun 2000;279:219–22.
47. Staab A, Loeffler J, Said HM, Diehlmann D, Katzer A, Beyer M, et al. Effects of HIF-1 inhibition by chetomin on hypoxia-related transcription and radiosensitivity in HT 1080 human fibrosarcoma cells. BMC Cancer 2007;7:213.
48. Dewangan J, Srivastava S, Mishra S, Pandey PK, Divakar A, Rath SK. Chetomin induces apoptosis in human triple-negative breast cancer cells by promoting calcium overload and mitochondrial dysfunction. Biochem Biophys Res Commun 2018;495:1915–21.
49. Waring P, Beaver J. Gliotoxin and related epipolythiodioxopiperazines. Gen Pharmacol 1996;27:1311–6.
50. Moerman KL, Chai CL, Waring P. Evidence that the lichen-derived scabrosin esters target mitochondrial ATP synthase in P388D1 cells. Toxicol Appl Pharmacol 2003;190:232–40.
51. Chatterji T, Keerthi K, Gates KS. Generation of reactive oxygen species by a persulfide (BnSSH). Bioorg Med Chem Lett 2005;15:3921–4.
52. Banik K, Harsha C, Bordoloi D, Lalduhsaki Sailo B, Sethi G, Leong HC, et al. Therapeutic potential of gambogic acid, a caged xanthone, to target cancer. Cancer Lett 2018;416:75–86.
53. Goode KM, Petrov DP, Vickman RE, Crist SA, Pascuzzi PE, Ratliff TL, et al. Targeting the Hsp90 C-terminal domain to induce allosteric inhibition and selective client downregulation. Biochim Biophys Acta Gen Subj 2017;1861:1992–2006.
54. Chen M, Ye K, Zhang B, Xin Q, Li P, Kong AN, et al. Paris Saponin II inhibits colorectal carcinogenesis by regulating mitochondrial fission and NF-κB pathway. Pharmacol Res 2019;139:273–85.
55. Beutler JA, Kashman Y, Pannell LK, Cardellina JH 2nd, Alexander MR, Balaschak MS, et al. Isolation and characterization of novel cytotoxic saponins from Archidendron ellipticum. Bioorg Med Chem 1997;5:1509–17.
56. Jia Z, Koike K, Ohmoto T, Ni M. Triterpenoid saponins from Ardisia crenata. Phytochemistry 1994;37:1389–96.
57. Dai LM, Huang RZ, Zhang B, Hua J, Wang HS, Liang D. Cytotoxic triterpenoid saponins from Lysimachia foenum-graecum. Phytochemistry 2017;136:165–74.
58. Mola MG, Nicchia GP, Svelto M, Spray DC, Frigeri A. Automated cell-based assay for screening of aquaporin inhibitors. Anal Chem 2009;81:8219–29.
59. Liptak A, Kusiak JW, Pitha J. Alkylating beta-blockers: activity of isomeric bromoacetyl alprenolol menthanes. J Med Chem 1985;28:1699–703.
60. Ni S, Chen X, Yu Q, Xu Y, Hu Z, Zhang J, et al. Discovery of candesartan cilexetic as a novel neddylation inhibitor for suppressing tumor growth. Eur J Med Chem 2020;185:111848.
61. See S, Stirling AL. Candesartan cilexetil: an angiotensin II-receptor blocker. Am J Health Syst Pharm 2000;57:739–46.
62. Francis BE, Swain C, Sabin V, Burns HD. Radioiodinated L-703,606: a potent, selective antagonist to the human NK1 receptor. Appl Radiat Isot 1994;45:97–103.
63. Jawien J, Gajda M, Rudling M, Mateuszuk L, Olszanecki R, Guzik TJ, et al. Inhibition of five lipoxygenase activating protein (FLAP) by MK-886 decreases atherosclerosis in apoE/LDLR-double knockout mice. Eur J Clin Invest 2006;36:141–6.
64. Abdali N, Parks JM, Haynes KM, Chaney JL, Green AT, Wolloscheck D, et al. Reviving antibiotics: efflux pump inhibitors that interact with AcrA, a membrane fusion protein of the AcrAB-TolC multidrug efflux pump. ACS Infect Dis 2017;3:89–98.
65. Hernlund E, Olofsson MH, Fayad W, Fryknäs M, Lesiak-Mieczkowska K, Zhang X, et al. The phosphoinositide 3-kinase/mammalian target of rapamycin inhibitor NVP-BEZ235 is effective in inhibiting regrowth of tumour cells after cytotoxic therapy. Eur J Cancer 2012;48:396–406.
66. Clement JA, Kitagaki J, Yang Y, Saucedo CJ, O'Keefe BR, Weissman AM, et al. Discovery of new pyridoacridine alkaloids from Lissoclinum cf. badium that inhibit the ubiquitin ligase activity of Hdm2 and stabilize p53. Bioorg Med Chem 2008;16:10022–8.

67. Wube AA, Gibbons S, Asres K, Streit B, Adams M, Bauer R, et al. *In vitro* 12(S)-HETE and leukotriene metabolism inhibitory activity of sesquiterpenes of Warburgia ugandensis. Planta Med 2006;72:754–6.
68. Kim KW, Sugawara F, Yoshida S, Murofushi N, Takahashi N, Curtis RW. Structure of malformin B, a phytotoxic metabolite produced by Aspergillus niger. Biosci Biotechnol Biochem 1993;57:787–91.
69. Bowden BF, Cusack BJ, Dangel A. 13-Epi-9-deacetoxyxenicin, a cytotoxic diterpene from the soft coral Asterospicularia laurae (Alcyonacea). Mar Drugs 2003;1:18–26.
70. Bewley CA, He H, Williams DH, Faulkner DJ. Aciculitins A−C: cytotoxic and antifungal cyclic peptides from the lithistid sponge Aciculites orientalis. J Am Chem Soc 1996;118:4314–21.